AGU PUBLICATIONS

JGR

Journal of Geophysical Research: Oceans

RESEARCH ARTICLE

10.1002/2015JC010744

Key Points:
- New observations of northward flow during northeast monsoon
- New drifter observations showing east India coastal current
- Northward flow and salinity intrusions

Correspondence to:
H. W. Wijesekera,
hemantha.wijesekera@nrlssc.navy.mil

Citation:
Wijesekera, H. W., T. G. Jensen, E. Jarosz, W. J. Teague, E. J. Metzger, D. W. Wang, S. U. P. Jinadasa, K. Arulananthan, L. R. Centurioni, and H. J. S. Fernando (2015), Southern Bay of Bengal currents and salinity intrusions during the northeast monsoon, *J. Geophys. Res. Oceans*, *120*, doi:10.1002/2015JC010744.

Received 21 JAN 2015
Accepted 25 SEP 2015
Accepted article online 1 OCT 2015

Southern Bay of Bengal currents and salinity intrusions during the northeast monsoon

H. W. Wijesekera[1], T. G. Jensen[1], E. Jarosz[1], W. J. Teague[1], E. J. Metzger[1], D. W. Wang[1], S. U. P. Jinadasa[2], K. Arulananthan[2], L. R. Centurioni[3], and H. J. S. Fernando[4]

[1]Naval Research Laboratory, Stennis Space Center, Mississippi, USA, [2]National Aquatic Resources Research and Development Agency, Colombo, Sri Lanka, [3]Scripps Institution of Oceanography, University of California, San Diego, California, USA, [4]Department of Civil Engineering, Environmental and Earth Sciences, University of Notre Dame, Notre Dame, Indiana, USA

Abstract Shipboard velocity and hydrographic profiles collected in December 2013 along with drifter observations, satellite altimetry, global ocean nowcast/forecast products, and coupled model simulations were used to examine the circulation in the southern Bay of Bengal as part of ongoing international research efforts in the region. The observations captured the southward flowing East India Coastal Current (EICC) off southeast India and east of Sri Lanka. The EICC was approximately 100 km wide, with speeds exceeding 1 m s^{-1} in the upper 75 m. East of the EICC, a subsurface-intensified 300 km-wide, northward current was observed, with maximum speeds as high as 1 m s^{-1} between 50 m and 75 m. The EICC moved low-salinity water out of the bay and the subsurface northward flow carried high-salinity water into the bay during typical northeast monsoon conditions during a time period when the central equatorial Indian Ocean was experiencing a westerly wind burst related to the Madden-Julian Oscillation (MJO) event. While the northward subsurface high-salinity flow has previously been observed during the southwest monsoon, it was observed during the northeast monsoon. The observations are consistent with northward high-salinity subsurface flow in numerical model solutions. The analysis suggests that direct forcing along the equator may play a significant role for high-salinity intrusions east of Sri Lanka.

1. Introduction

Current and hydrographic profiles collected in December 2013 along with satellite altimetry and drifter observations, model nowcast/forecast products, and model simulations were used to examine the circulation in the southern Bay of Bengal (BoB) during the northeast monsoon. The observations were made during a mooring deployment cruise in the southern BoB using the research vessel Roger Revelle. Throughout the duration of the cruise, the regional wind conditions consisted of northeasterly winds over the BoB as commonly present during the northeast monsoon and a westerly wind burst (WWB) over the west-central part of the equatorial Indian Ocean (IO).

The study is a collaborative effort (2013–2017) between the Effects of Bay of Bengal Freshwater Flux on Indian Ocean Monsoon (EBOB) program of the U.S. Naval Research Laboratory, the Air-Sea Interactions in Northern Indian Ocean-regional initiative (ASIRI) of the U.S. Office of Naval Research, the Ocean Mixing and Monsoons (OMM) Mission of India, and the Coastal Currents Observations Program (CCOP) of Sri Lanka [*Lucas et al.*, 2014]. One of the major objectives of ASIRI-EBOB is to understand and to quantify dynamical processes and boundary transports that control fresh and salt water exchanges between the BoB and the Arabian Sea (AS).

The monsoon-driven reversing currents control the freshwater balance of the BoB by flushing out low-salinity water from the bay and by bringing saltier water into the bay. The BoB circulation is strongly controlled by wind forcing and remote forcing mechanisms [*Schott and McCreary*, 2001; *Shankar et al.*, 2002; *Vialard et al.*, 2009]. However, both the freshwater and equatorial dynamics can affect the entire BoB. The East India Coastal Current (EICC) [e.g., *Shetye et al.*, 1996], which transports low-salinity BoB water during the late fall and early winter months (November–January) flows southward along the eastern boundaries of India and Sri Lanka, and then westward along the southern coast of Sri Lanka before entering the southeast

AS [*Cutler and Swallow*, 1984; *Rao et al*., 1989; *Schott et al*., 1994; *Shetye et al*., 1996; *McCreary et al*., 1996; *Jensen*, 2001; *Han and McCreary*, 2001; *Durand et al*., 2009; *Mukherjee et al*., 2014]. During the winter monsoon, both the EICC and the westward flowing Winter Monsoon Current (WMC) south of Sri Lanka transport much of the low-salinity water toward the AS [*Cutler and Swallow*, 1984; *Rao et al*., 1989; *Schott et al*., 1994; *Shetye et al*., 1996]. *McCreary et al*. [1996] used a linear numerical ocean model based on vertical mode separation to quantify the processes in the BoB. During the boreal winter, the southward EICC is primarily driven by local longshore winds, while interior Ekman pumping drives a surface northward flow near 85°E, with some influence of remote forcing from the equator.

It has been recognized that the major influx of saltier water into the bay is via the Summer Monsoon Current (SMC), which flows eastward from the AS into the southern BoB during the southwest monsoon [*Murty et al*., 1992; *Schott and McCreary*, 2001; *Han and McCreary*, 2001; *Jensen*, 2001, 2003; *Vinayachandran et al*., 2013]. Transition periods (April–May and September–October) between the two monsoons are associated with WWBs [e.g., *Wyrtki*, 1973], some of which relate to Madden-Julian Oscillation (MJO) events [*Madden and Julian*, 1971, 1972; *Zhang*, 2005; *Chi et al*., 2014; *Moum et al*., 2014]. WWBs force strong eastward surface currents along the equator [e.g., *Yoshida*, 1959; *Wyrtki*, 1973; *Iskandar and McPhaden*, 2011; *Nagura and McPhaden*, 2012]. The equatorial jet, referred to as "the Wyrtki Jet," appears semiannually during the monsoon transition periods [*Wyrtki*, 1973; *O'Brien and Hurlburt*, 1974; *Knox*, 1974; *Iskandar and McPhaden*, 2011; *Nagura and McPhaden*, 2010, 2012; *Joseph et al*., 2012]. During WWBs, the ocean response is a rapid eastward equatorial jet in the mixed layer and often an equatorial symmetric Rossby wave to the west of the jet. A deepening of the thermocline is caused by convergence on the equator in the jet region and an off-equator shallowing of the thermocline to the west is caused by divergence associated with the Rossby wave [*O'Brien and Hurlburt*, 1974]. The equatorial thermocline anomaly is known to propagate eastward with a phase speed close to that of a free equatorial Kelvin wave, and upon reaching the Sumatra coast, it partly reflects as a symmetric equatorial Rossby wave and two poleward moving coastal Kelvin waves [e.g., *Anderson and Rowlands*, 1976; *Cane and Sarachik*, 1977; see also *Philander*, 1990, pp. 126–128]. High frequency northward moving Kelvin waves can propagate along the coast and influence the circulation in the Bay of Bengal. Analysis of satellite SSH and direct current measurements along the east coast of India indicate that upper ocean flow field, especially near 15°–19°N, has strong intra-seasonal oscillations of alongshore currents [*Vialard et al*., 2009; *Mukherjee et al*., 2014]. These oscillations represent sea-level fluctuations in the northern Indian Ocean, specifically in the equatorial and in the coastal wave guides and are likely a result of MJO events [*Vialard et al*., 2009]. The low frequency poleward propagating Kelvin waves subsequently radiate as Rossby waves from the eastern boundary into the interior of the ocean [*Anderson and Rowlands*, 1976]. In the case of the Bay of Bengal these Rossby waves propagate across the bay to the East Indian Coast [*Yu et al*., 1991; *Potemra et al*., 1991; *McCreary et al*., 1993]. This is the classical remote forcing of the BoB by equatorial waves.

Here we examine currents in the southern BoB observed in December 2013 during the northeast monsoon, including boundary currents and a northward flow in the interior of the southern BoB. Plausible connections of currents in the BoB to the equatorial flow field are demonstrated through analysis of output from numerical models. The paper is organized as follows. In section 2, platforms, measurements, and models are described. Section 3 describes wind observations, currents and hydrography, and model comparisons. A discussion is given in section 4, and major findings are summarized in section 5.

2. Measurements and Models Description

Data from acoustic Doppler current profilers (ADCPs) and a conductivity, temperature and depth (CTD) sensor were collected during 17–24 December 2013 from the R/V Roger Revelle operating out of Colombo, Sri Lanka. Current measurements were made using two hull-mounted Teledyne RDI 150 kHz and 75 kHz ADCPs. Three minute averaged velocity profiles were recorded. Shallowest and deepest ADCP bins were 29 m and 800 m for 75 kHz measurements, and were 21 m and 300 m for 150 kHz measurements. Time-depth sections of currents in the southern BoB were collected approximately along 5.25°N during the outbound and inbound transects between Sri Lanka and the mooring site at 5.25°N, 85.5°E. Data for the first transect were collected over 21 h between 82°E and 85.5°E on 17 and 18 December (T18, blue line in Figure 1a), and for the second transect over 35 h between 80°E and 85.5°E on 23 and 24 December (T24, red line in Figure 1a). A few CTD

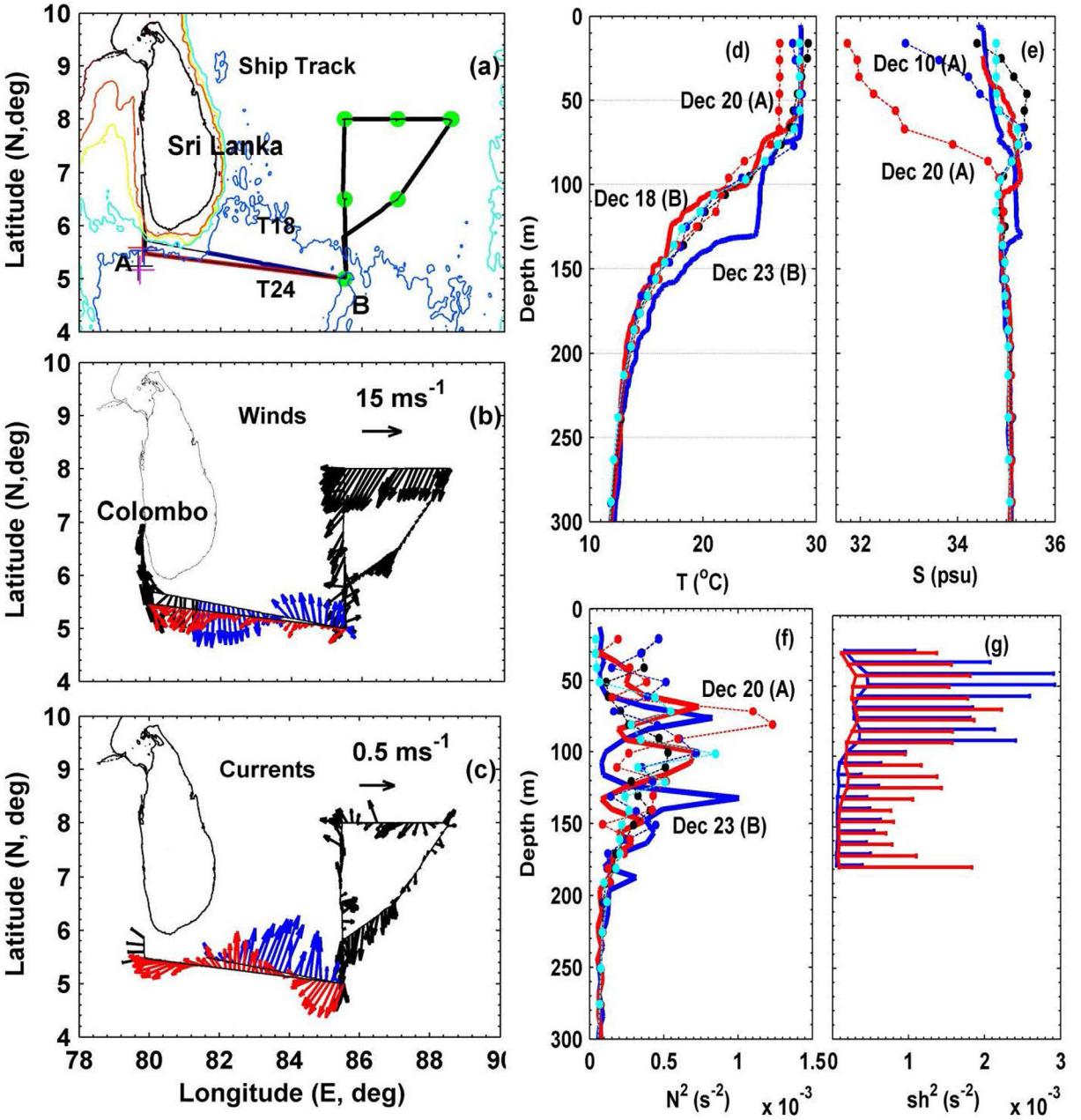

Figure 1. (a) R/V *Roger Revelle* tracks. The thick blue line, T18 is the ship-transect on 18 December 2013, and the thick red line, T24 is the ship-transect on 23 and 24 December. The thick black lines indicate the ship track during mooring deployment, where the green dots represent the mooring and CTD locations. The ARGO-CTD and ship-CTD locations are marked in A and B respectively. Thin red, yellow, cyan, and blue lines are, respectively, 1000 m, 2000 m, 3000 m, and 4000 m bathymetry contours. (b) Wind vectors based on hourly averages along the ship track. Blue and red arrows denote winds along T18 and T24, respectively. (c) Upper 175 m depth averaged ADCP current vectors along the ship track. (d) Temperature and (e) salinity profiles at B (thick solid lines) and at A (dashed lines with dots). The thick red and blue lines are the CTD profiles taken on 18 and 23 December 2013, respectively. The dotted cyan, blue, red, and black lines are the ARGO-CTD profiles taken on 30 November, 10, 20, and 30 December. (f) Profiles of buoyancy frequencies squared (N^2) estimated from ARGO-CTD profiles (dashed lines with dots) at A, and from ship-CTD profiles for 18 December (blue) and 23 December (red) at B. (g) Squared shear of horizontal currents averaged along T18 (blue) and T24 (red) with maximum values (horizontal lines).

profiles were collected at the mooring locations (Figures 1a, 1d, and 1e). Underway temperature (T) and salinity (S), at depths of about 5 m below the sea surface, and meteorological observations (Figure 1b) were also recorded at 15 s intervals.

Several satellite-tracked surface-drifters were deployed during October–December 2013 (Table 1). The majority were deployed off the east coast of Sri Lanka. Each drifter was equipped with a GPS transmitter

Table 1. Deployed Location and Time for Drifters Shown in Figure 4

ID	Deployment Time	Longitude (°E)	Latitude (°N)
A	24 Oct 2013, 15:45:00	82.0949	8.8334
B	24 Oct 2013, 23:30:00	83.5510	9.96605
C	21 Nov 2013, 05:16:00	86.8526	16.2226
D	26 Nov 2013, 04:30:00	82.6353	7.6234
E	21 Dec 2013, 00:15:00	81.8739	7.6495
F	23 Dec 2013, 05:16:00	81.3051	9.2361
G	23 Dec 2013, 06:16:00	81.3109	9.4795
H	23 Dec 2013, 08:17:00	81.3004	8.9492

and a thermistor, and recorded position and sea surface temperature (SST) every 15 min. Drifter tracks were used to examine flow patterns and speeds of boundary currents around Sri Lanka.

Maps of vectors representing the sum of geostrophic and Ekman velocity fields at 15 m depth were constructed by running a 2-D linear fit between the drifter and the near real-time daily AVISO (Archiving, Validation and Interpretation of Satellite Oceanographic) velocity data to obtain the mean, time-independent, velocity field [*Centurioni et al*., 2008]. Using a least-square model, we calculate a location-dependent slope parameter, which is used to add back the time-dependent part of the geostrophic flow anomaly as computed from the AVISO altimetry. NCEP (National Centers for Environmental Prediction) reanalysis winds were used to compute the Ekman currents [*Ralph and Niiler*, 1999]. Tides, near-inertial and any other ageostrophic motions were not included in this representation of the near-surface currents, which have an inherent resolution of 1/3° and 24 h, the spatial and temporal resolutions of the near real-time AVISO product. Slippage of drifters is quantified as 1 cm s^{-1} for a 10 m s^{-1} wind speed [*Niiler et al*., 1995], and velocities of drifters without drogues were recovered using the method described in *Pazan and Niiler* [2001].

The model output from the U. S. Navy's operational global ocean nowcast/forecast system and the NRL's Coupled Ocean-Atmosphere Mesoscale Prediction System (COAMPS^{TM}) were used to examine currents, and temperature and salinity fields in the BoB during December 2013. The global ocean system is presently composed of the 1/12° HYbrid Coordinate Ocean Model (HYCOM) (~9 km horizontal resolution in the equatorial Indian Ocean and BoB) and the Navy Coupled Ocean Data Assimilation (NCODA) system. The HYCOM nowcast/forecast system produces nowcasts and forecasts of ocean conditions including three-dimensional ocean temperature, salinity, and current structure; surface mixed layer depth; and the location of mesoscale features such as eddies, meandering currents, and fronts [*Metzger et al*., 2014]. Presently, surface satellite measurements (e.g., sea surface height and SST) are projected into the ocean using vertical correlations between surface expressions and subsurface fields to be used in a 3-D analysis. The method, referred to as the Modular Ocean Data Assimilation System (MODAS) [*Fox et al*., 2002] is part of NCODA. Recently the method has been improved through the Improved Synthetic Ocean Profile (ISOP) scheme [*Helber et al*., 2013]. Available hydrographic observations from XBTs, CTDs gliders and Argo floats are used to determine mismatches in model forecasts, leading to model corrections according to error covariances. However, the sparse historical data used to compute ISOP may not adequately sample the scales arising near coastal boundaries and over steep ridges.

The NRL COAMPS is a fully three-way-coupled model (atmosphere/surface waves/ocean) and has been set up for the BoB with 6 km resolution for the atmosphere with 60 vertical levels and uses the three-dimensional NRL Atmospheric Variational Data Assimilation System (NAVDAS) [*Daley and Barker*, 2001]. For the ocean, it has 2 km resolution with 60 vertical levels and 0.5 m vertical resolution within the upper 10 m. NAVDAS incorporates satellite data, weather radar data, aerosonde profiles, and surface meteorology to provide a realistic atmosphere. An analysis that updates the atmospheric model solution with observations is done every 12 h to ensure realistic atmospheric condition during the coupled model simulation. The ocean model is the Navy Coastal Ocean Model (NCOM) and includes 8 diurnal and semidiurnal tidal components [*Martin*, 2000]. Data assimilation was not used in this study. The wave model is Simulating Waves Nearshore (SWAN) [*Booij et al*., 1999] and has a spatial resolution of 1/8° with 33 spectral bands and 48 directions for each frequency. The surface wave field provides a feedback to the upper ocean through Stokes drift in the turbulence closure scheme [*Kantha and Clayson*, 2004], while feedback from the ocean to the wave field is through surface currents and sea level. The three model components exchange information with a 6 min coupling interval. Initial conditions and 3 hourly boundary conditions for COAMPS are supplied by the global nowcast/forecast system for the ocean and by the Navy Global Environmental Model (NAVGEM) developed by NRL for the atmosphere. The COAMPS model domain ranges from 69.5°E to 99.1°E zonally, and from 1.5°S to 22.9°N meridionally.

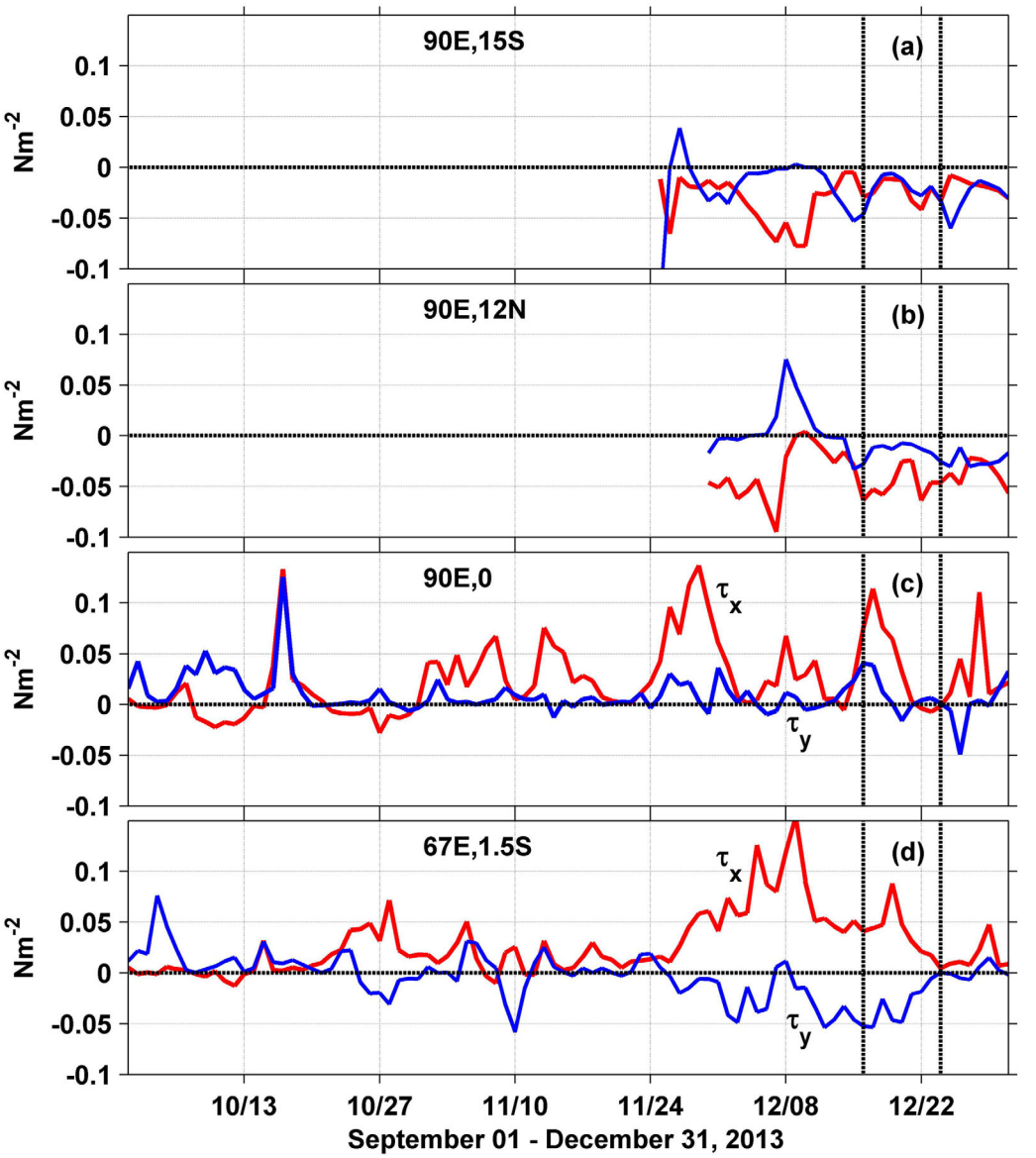

Figure 2. Wind stress components (N m^{-2}) measured by sensors mounted on RAMA moorings at the northern BoB and the equatorial Indian Ocean (http://www.pmel.noaa.gov/tao/data_deliv/). (a) 90°E, 15°N, (b) 90°E, 12°N, (c) 90°E, 0°, and (d) 67°E, 1.5°. Zonal (τ_x) and meridional (τ_y) components are marked in red and blue, respectively. The two vertical dashed lines at 17 and 24 December 2013 denote the starting and ending days of our measurements.

3. Results

3.1. Background Meteorology

Winds, measured by the ship-mounted sensors, were predominantly from the north and northeast, with magnitudes varying from 2 to 15 m s^{-1} (Figure 1b). Similar northeasterly winds were recorded by meteorological sensors mounted on buoys at 90°E, 12°N, and 90°E, 15°N (Figure 2), as part of the Research Moored Array for African-Asian Monsoon Analysis and Prediction (RAMA) [*McPhaden et al.*, 2009]. The RAMA buoys in the central equatorial Indian Ocean recorded a westerly wind burst starting near the end of November 2013 (Figure 2) that lasted more than three weeks with a daily averaged wind stress as large as 0.15 N m^{-2} (wind speed ~10 m s^{-1}). The weekly averaged satellite products from the Tropical Rainfall Measuring Mission's (TRMM) Microwave Imager (TMI) (www.remss.com) showed that the wind event (> 5 m s^{-1}) occurred over an area covering 55°E to 90°E, zonally, and from 1°N to 5°S, meridionally, with convective activities during 7–14 December. The analyses of NCEP (http://www.cpc.ncep.noaa.gov/products/precip/CWlink/MJO/)

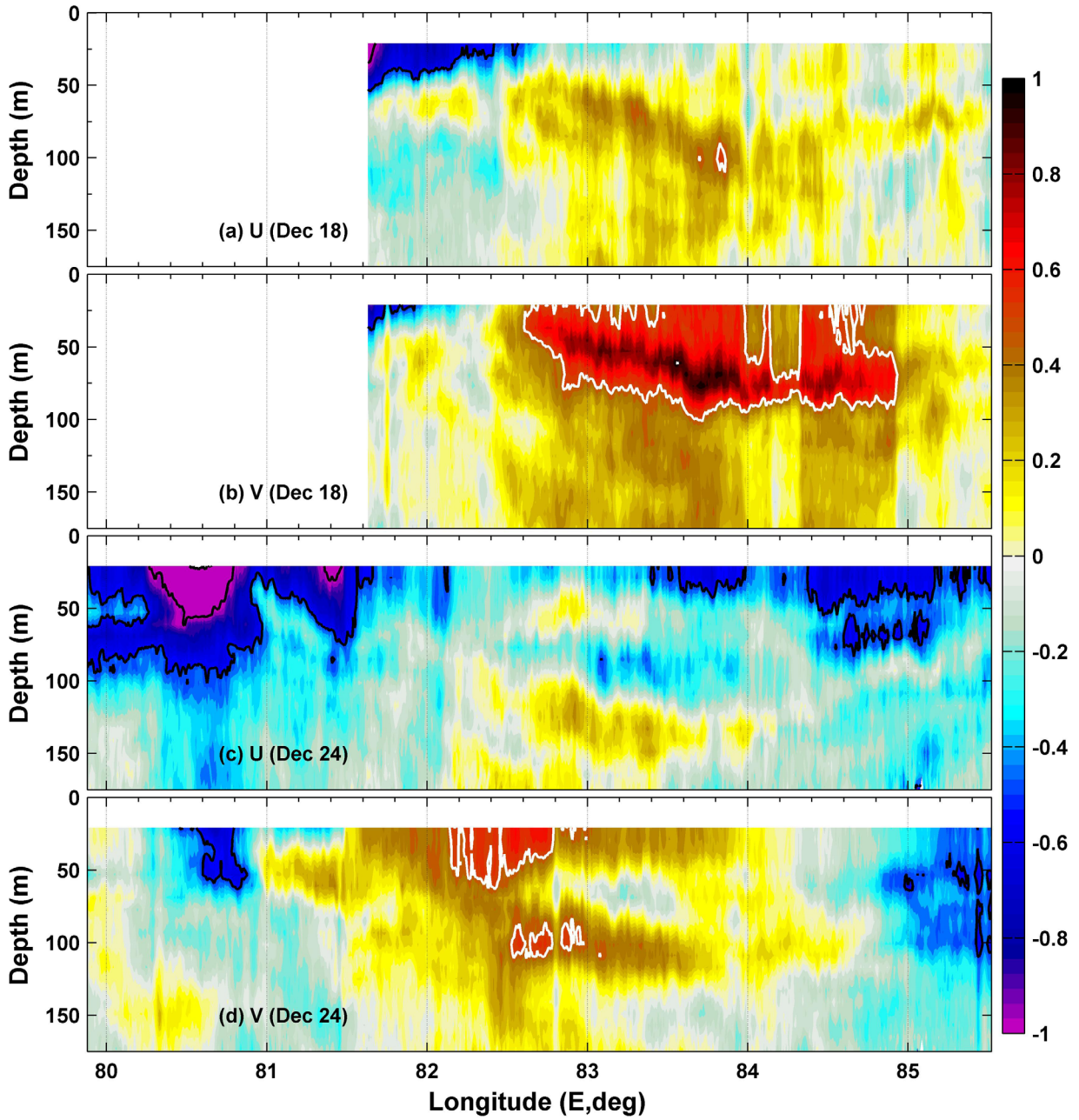

Figure 3. Velocity along (a, b) T18 and (c, d) T24. T18 and T24 tracks are shown in Figure 1a. Sections of (a, c) zonal velocity, U and (b, d) meridional velocity, V. Velocities are in m s^{-1}. Velocity contours of –1 m s^{-1} and –0.5 m s^{-1} are marked in black lines and contours of +0.5 m s^{-1} are marked in thick white lines.

and by the Australian Bureau of Meteorology (http://www.bom.gov.au/climate/mjo/) indicate that the westerly wind anomaly was associated with a MJO event and moved from west to east during December 2013. Wind products from the European Centre for Medium Range Weather Forecasting Integrated Forecast System (ECMWF) illustrate similar wind events along the equator and northeasterly winds over the BoB. As mentioned above, these WWBs generate eastward flowing equatorial jets [e.g., *Moum et al.* 2014; *Chi et al.*, 2014] that can play a major role in the dynamics of the southern BoB. Plausible impacts of these jets will be addressed in section 4.

3.2. Observations of East India Coastal Current (EICC)

Velocities are shown in Figures 1c and 3 for outbound T18 (18 December) and inbound T24 (23 and 24 December) transects which were approximately along 5.25°N. The west-southwestward flowing EICC is well

Table 2. Near Surface Velocity From Drifter Tracks Shown in Figure 4[a]

ID	Time Averaging Interval: Starting and Ending of Drifter Segments in UTC	U (std) (m s^{-1})	V (std) (m s^{-1})	Speed (m s^{-1})
	East of India: Averaging Box: Lon. 79.8–81.3°E, Lat. 10.5–14.5°N			
A	19-11-2013, 04:00:00 to 25-11-2013, 17:30:00	−0.11 (0.17)	−0.76 (0.34)	0.77
B	24-11-2013, 10:15:00 to 29-11-2013,23:45:00	0.09 (0.22)	−0.98 (0.19)	0.98
C	10-12-2013, 01:00:00 to 13-12-2013, 22:30:00	−0.17 (0.61)	−1.28 (0.28)	1.29
	East of Sri Lanka: Averaging Box: Lon. 80.5–82.5°E, Lat. 6.5–10.5°N			
A	25-11-2013, 17:45:00 to 29-11-2013, 09:15:00	0.46 (0.18)	−0.80 (0.14)	0.92
B	29-11-2013, 16:15:00 to 6-12-2013, 15:30:00	0.22 (0.14)	−0.74 (0.23)	0.77
C	13-12-2013, 22:45:00 to 17-12-2013, 15:45:00	0.51 (0.38)	−1.38 (0.19)	1.47
E	21-12-2013, 00:15:00 to 22-12-2103, 03:15:00	0.07 (0.23)	−1.30 (0.19)	1.30
F	23-12-2013, 05:16:00 to 27-12-2103, 12:16:00	0.19 (0.21)	−0.82 (0.15)	0.84
G	23-12-2013, 06:16:00 to 27-12-2013, 21:16:00	0.29 (0.15)	−0.83 (0.10)	0.88
H	23-12-2013, 08:17:00 to 27-12-2013, 04:32:00	0.22 (0.21)	−0.82 (0.12)	0.85
	South of Sri Lanka: Averaging Box: Lon. 79.8–81.3°E, Lat. 4.0–6.5°N			
D	30-11-2013, 01:50:00 to 1-12-2013, 22:30:00	−1.01 (0.04)	0.04 (0.22)	1.01
B	7-12-2013, 13:30:00 to 8-12-2013, 23:45:00	−1.34 (0.08)	0.15 (0.20)	1.35
C	18-12-2013, 18:00:00 to 20-12-2013, 09:45:00	−1.16 (0.09)	−0.33 (0.22)	1.21
E	23-12-2013, 00:30:00 to 24-12-2013, 16:00:00	−1.16 (0.09)	−0.43 (0.20)	1.24
F	28-12-2013, 12:31:00 to 30-12-2013, 19:01:00	−0.84 (0.10)	−0.04 (0.21)	0.84
G	30-12-2013, 19:01:00 to 1-1-2014, 14:16:00	−1.06 (0.12)	−0.06 (0.15)	1.06
H	28-12-2013, 06:32:00 to 29-12-2014, 22:17:00	−1.15 (0.09)	−0.06 (0.22)	1.15
	West of Sri Lanka: Averaging Box: Lon. 74.0–79.8°E, Lat. 4.0–8.0°N			
D	1-12-2013, 01:00:00 to 9-12-2013, 19:45:00	−0.90 (0.27)	0.22 (0.29)	0.93
B	8-12-2013, 07:15:00 to 2-2-2014, 05:00:00	−0.15 (0.34)	0.00 (0.27)	0.15
C	19-12-2013, 15:45:00 to 27-12-2013, 03:15:00	−1.11 (0.20)	0.06 (0.19)	1.11
E	23-12-2013, 20:45:00 to 29-12-2013, 17:00:00	−1.36 (0.27)	−0.06 (0.27)	1.36
F	29-12-2013, 17:01:00 to 11-1-2014, 23:01:00	−0.58 (0.18)	0.06 (0.26)	0.58
G	31-12-2013, 19:46:00 to 10-1-2014, 22:01:00	−0.82 (0.26)	0.09 (0.36)	0.82
H	29-12-2013, 04:17:00 to 12-1-2014, 01:47:00	−0.57 (0.33)	0.04 (0.38)	0.57

[a]The initial locations are given in Table 1. Zonal (U) and meridional (V) velocity components were averaged into four geographical regions representing south-east of India, east of Sri Lanka, south of Sri Lanka, and west of Sri Lanka. Standard deviations are given in parenthesis.

captured during the inbound transect (Figures 1c, 3c, and 3d). The EICC at 21 m depth had a core velocity greater than 1.6 m s^{-1}, and was about 100 km wide. Stronger velocities ($>$ 0.5 m s^{-1}) were limited to the upper 100 m, and velocities as large as 0.2 m s^{-1} extended to a depth of about 250 m. Velocities were expected to be more intense near the surface but could not be measured by shipboard ADCP instruments. The outbound transect appears to have just clipped the eastern edge of the EICC (Figures 3a and 3b).

There were no shipboard-hydrographic measurements along these transects to examine the T-S variability and the strength of density stratification within the EICC and the outside flow field. Therefore we used ship CTD profiles, collected during 18 and 23 December at 5.25°N, 85.5°E, and CTD profiles from ARGO floats on November–December along the ship transect (Figure 1). Four ARGO-CTD profiles (WMO: 2901620) were found on 30 November, 10, 20, and 30 December at (5.236°N, 79.673°E), (5.534°N, 79.838°E), (5.585°N, 79.793°E), and (5.162°N, 79.719°E), respectively (http://argoweb.whoi.edu/argo_database_web/index.html?wmo=2901620). The locations of ARGO-CTD profiles (Figure 1a) were close to the core of the EICC (Figure 3c). The CTD profiles shown in Figures 1d and 1e capture the low-salinity, low-temperature signature of the EICC near 5.59°N, 79.8°E, where the temperature in the upper 75 m was nearly uniform at about 26.5°C, and the salinity increased from 31.8 psu at 20 m to 35 psu at 100 m. The density stratification was stronger within the EICC due to low-salinity effects as compared to outside of EICC (Figure 1f).

The EICC was well developed off the coasts of India and Sri Lanka during November–December 2013 (Figure 4 and Table 2). The drifters (D-H), deployed in November and December 2013 within 100 km of the Sri Lankan shelf (Figure 4), moved southward before turning westward as they passed south of Sri Lanka. The drifters (A-C), deployed away from the Sri Lankan and Indian shelf in late October and November 2013 moved north/northwestward, merged with the EICC over the continental slope of India, and then moved equatorward along the eastern boundary (Figure 4). The movement of drifters toward the Indian shelf is consistent with a north/northwestward geostrophic recirculation resulting from the mesoscale eddy field. The EICC was weak between 16.5°N and 19°N, but became strong ($>$1 m s^{-1}) south of 16.5°N (Figure 4). The EICC was confined to a narrow boundary current southeast of India and east of Sri Lanka, and later developed into an approximately 200 km-wide current as it turned westward south of Sri Lanka (Figures 4 and 5). The majority of

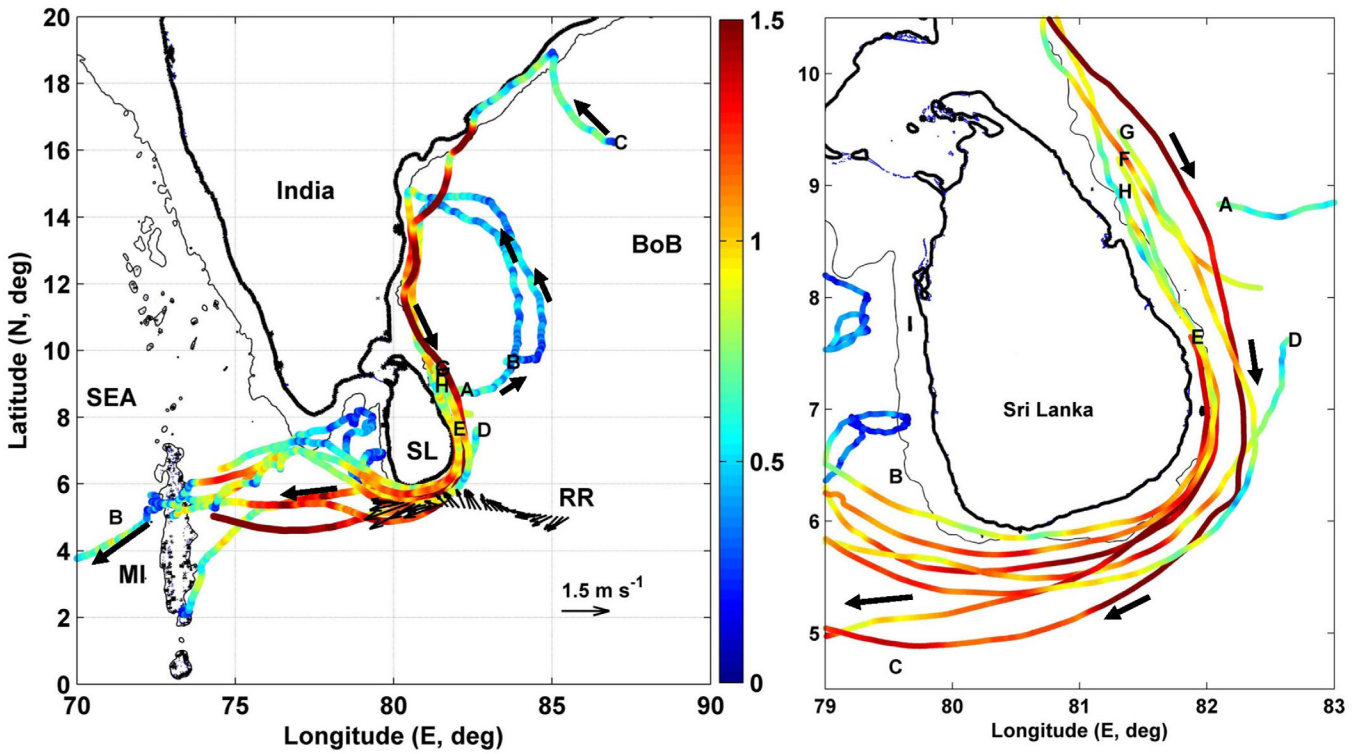

Figure 4. Tracks of eight drifters deployed east of Sri Lanka and southern BoB between 24 October and 23 December 2013. Initial location and time of these drifters are given in Table 1. (left) Drifter tracks (A-H), and the corresponding speeds (color shading) in m s^{-1}. The thick black arrows marked on drifter trajectories show the direction of the flow. The thin black arrows indicate velocity vectors at 21.5 m depth along T24 (Figure 1) on 23 and 24 December 2013 from the R/V Roger Revelle (RR) mounted 150 kHz ADCP. (right) Enlarged view of drifter tracks and speeds around Sri Lanka. SL, MI, and SEA denote Sri Lanka, Maldives Island chain, and Southeast Arabian Sea, respectively. The thin black line represents 1000 m bathymetry contour.

drifters deployed in the southern BoB ended up on the shallow shelf off the eastern coast of the Maldives Island chain. Two drifters (B, C) out of 8 passed through shallow narrow gaps in the topography near 5.5°N, 73°E. Drifter, B ventured into the Arabian Sea and indicates that the BoB water moves through the gaps in

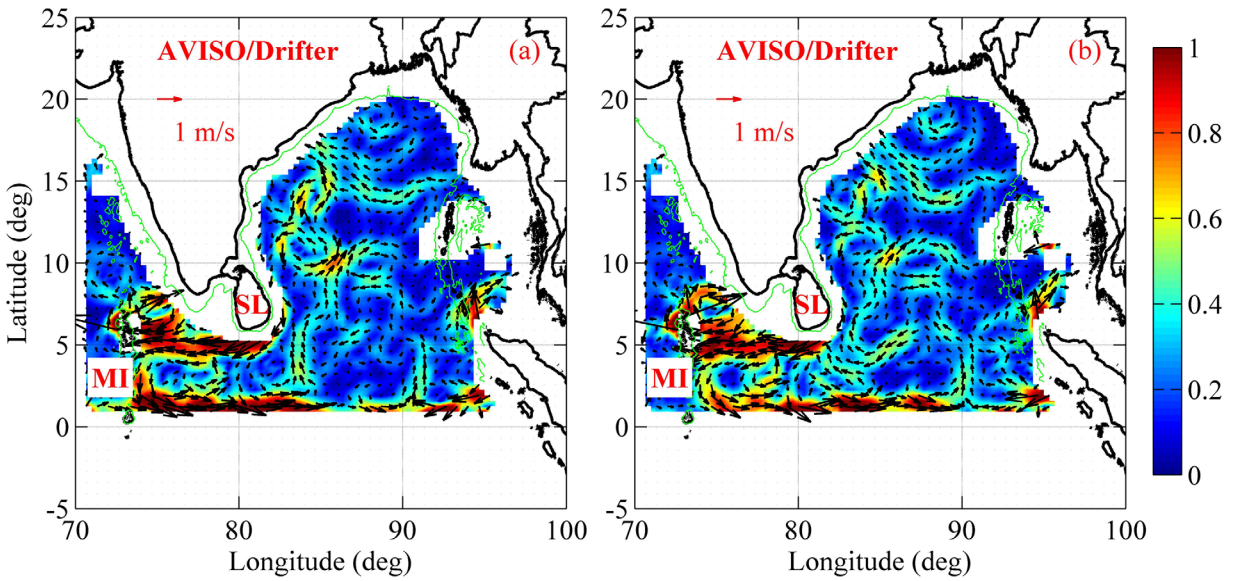

Figure 5. Surface current vectors (arrows) at 15 m depth along with their magnitudes (color shading) from combined AVISO and drifter products for (a) 18 December 2013 and (b) 24 December 2013. Velocities are in m s^{-1}. MI denotes Maldives Island Chain and SL denotes Sri Lanka.

Maldives Island chain (Figure 4). Drifter, G moved equatorward along the island chain. On average, the speed of the EICC was about 1 m s^{-1} between southeast Indian and Sri Lankan shelves (16.5°N, 6°N) and close to the Maldives Island chain (~74°E, 5.5°N), although instantaneous speeds were as large as 1.5 m s^{-1}.

The maps of near-surface currents (Figure 5) show a well-developed westward current south of Sri Lanka, and meandering currents and mesoscale features in the south-central BoB and south of Sri Lanka. The AVISO-drifter products only partially resolved coastal boundary currents east of India and Sri Lanka due to limitations of the analysis. The basic near-surface features are qualitatively similar to drifter observations and the combined AVISO drifter products (Figures 3–5).The AVISO-drifter currents did not always capture the detailed spatial and temporal variability which was possibly due to the smoothness of the AVISO product, inaccuracies of the Ekman model and the near real-time version of the altimetry data set, and the absence of tides and inertial waves. Nevertheless drifter/altimetry derived products provided reasonable estimates of the near surface velocity.

3.3. Observations of Northward Flow

To the east of EICC, there is a north-northeastward flow about 300 km wide with current speeds that exceed 0.5 m s^{-1} at depths down to about 100 m and with near-surface maximum velocities that exceed 1 m s^{-1} in the core (Figure 3). There is a subsurface velocity maximum for the outbound leg located between 50 and 100 m. The subsurface maximum is about 20 m deeper but weaker on the inbound leg. There appears to be eddy activity on the eastern end of the transect as indicated by the ADCP current vectors (Figure 1c). Velocity shear is large and maximum values of the squared shear range up to 3×10^{-3} s^{-2} (Figure 1g). AVISO-drifter currents shown in Figure 5 further illustrate a ribbon-like, ~200 km wide, northward flow extending from 1°N to about 12°N between 83°E and 85°E to the east of the EICC, and is consistent with ADCP currents. This provides a further qualitative validation of the AVISO-drifter analysis.

The CTD profiles, collected on 18 and 23 December at 5.25°N, 85.5°E, and ARGO-CTD profiles, collected on 30 November, 10, 20, and 30 December at 5.2°N, 79.8°E, were used to compute the density stratification. These CTD profiles near 5.25°N, 85.5°E are consistent with historical records for the month of December (not shown in Figure 1).The temperature in the upper 60–70 m was nearly uniform but the salinity in the upper 100–125 m was stratified (Figures 1d and 1e) with a maximum between 50 and 125 m. It is noteworthy that the subsurface salinity maximum exceeding 35 psu is also seen in the historical November–December CTD profiles (not shown in Figure 1). This indicates that the subsurface high salinity intrusion may be a common occurrence rather than a unique event. The density stratification was strong between 30 m and 190 m (Figure 1f), where the mean buoyancy-frequency squared (N^2) was about 3×10^{-4} s^{-2}. The buoyancy frequency is same order of magnitude as the velocity shear of horizontal currents (Figures 1f and 1g).

3.4. Model Results

The global model HYCOM and the regional model COAMPS captured the basic features of the flow, including the EICC, eddies, and a narrow-band of northward flow (Figures 6–8). Figure 6 displays longitude-depth sections of meridional currents and salinity for 18 December 2013, along the eastern boundary of India and Sri Lanka. The low-salinity (<33.5 psu) water occupied the upper 50 m of the BoB. The salinity below 50 m was greater than 35 psu, but salinity higher than 35.5 psu was confined to approximately a 50 m thick layer between depths of 50 m and 125 m. Maps of velocity and salinity fields from both COAMPS and HYCOM (Figures 7) further display the boundary current at different depths, and lateral spreading and meandering of high-salinity water in the interior of the southern BoB. Both the COAMPS and HYCOM models show a convergence zone near 82°E of strong eastward equatorial flow to the west of that longitude and strong westward flow east of that longitude. Near the surface (Figures 7a and 7c) the converging flow near 82°E is from the southwest as well as from the southeast and has salinity close to 34 psu. At depth (Figures 7b and 7d), the northward flow is primarily from the southwest with salinity 35 psu or higher. The northward flow of low salinity water near the surface and high salinity water at depth span the 10 day model simulation and are associated with the equatorial convergence.

Longitudinal-depth sections of U, V, and S along the 5.28°N illustrate the low-salinity core of the EICC, the westward flow between south of Sri Lanka and Maldives Islands, and a layer of high-salinity in the pycnocline (Figure 8). Both models captured the basic features of the EICC qualitatively. But differences in strength and structure are evident in the interior and subsurface flow field. The model results illustrate that

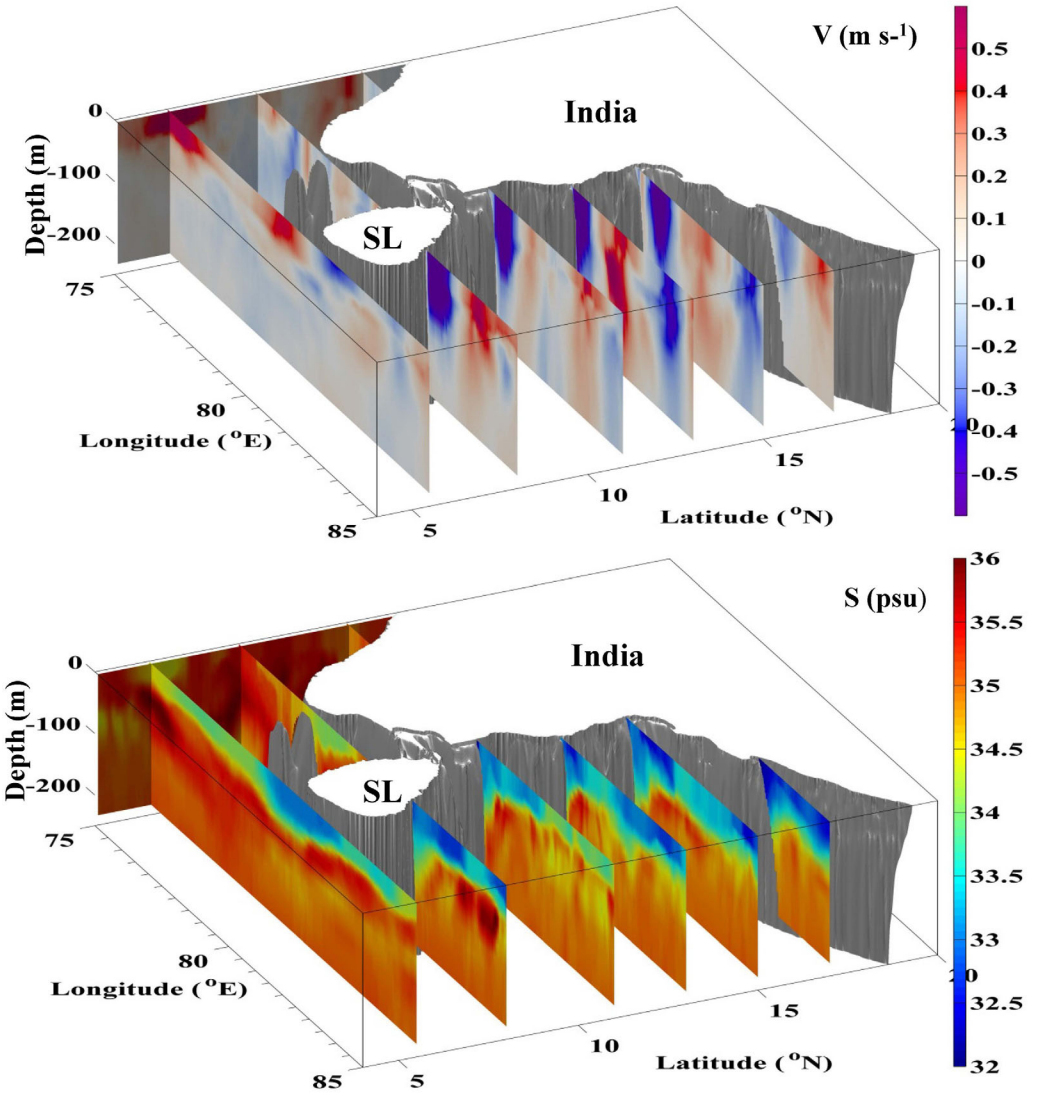

Figure 6. The daily averaged COAMPS sections of meridional velocity (top) and salinity (bottom) for 18 December 2013. The slices are along 75.1°E and 5.5°N, 8°N, 11°N, 13°N, 15°N, and 17°N.

the low-salinity water in the upper 100 m flowed equatorward along the eastern boundaries of India and Sri Lanka while higher salinity in the interior of the bay flowed northward (Figures 6–8). The modeled boundary current was weak north of 17°N, but it became quasi-steady south of 16°N. The EICC off India and east of Sri Lanka was approximately 100 m deep and 100 km wide with a magnitude of about 1 m s^{-1}. The EICC bent westward following the coast line as it passed south of Sri Lanka.

The models further indicate broadening of the EICC once it passed south of Sri Lanka as indicated by drifters and AVISO-drifter currents (Figures 6–8). The westward moving flow was topographically steered by the Maldives Island chain (Figure 7). Here the flow bifurcates into a northward branch and a southward branch that are connected to the eastward flow near 2°N. A fraction of the westward flow entered the southern AS through gaps in Maldives Island chain (Figure 7). Implementation of small islands and gaps in COAMPS and HYCOM is not identical, and therefore we can expect differences in modeled flow fields near the Maldives Islands. Both products showed plumes of low-salinity water passing through shallow and narrow gaps in the bathymetry (Figures 7c and 7d) similar to the drifter trajectory (B) shown in Figure 4. The gaps in HYCOM are deeper and narrower than in COAMPS, resulting in narrower, more intense and deeper through-flow than COAMPS, which has a wider and slower flow.

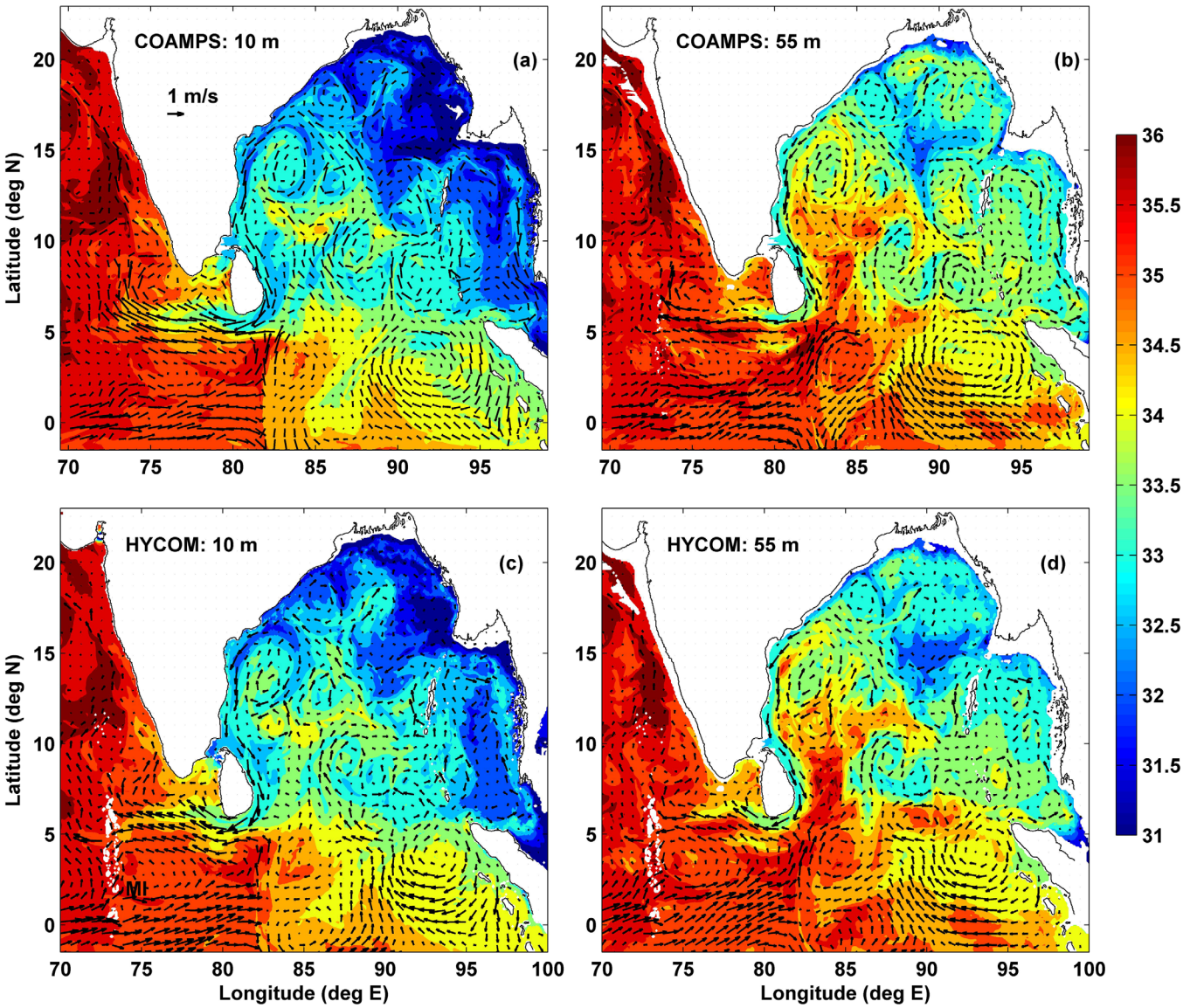

Figure 7. (top) COAMPS velocity vectors (arrows) and salinity (psu) (color shading) at (a) 10 m and (b) 55 m on 18 December 2013. (bottom) HYCOM velocity vectors (arrows) and salinity distribution (psu) (color shading) at (c) 10 m, and (d) 55 m. MI denotes Maldives Island chain.

The high-salinity equatorial flow, found between the southern-edge of the Maldives Islands (~2°N) and just south of the equator (4°S, not shown in Figures 7 and 8), bifurcates near 82°E-84°E, and the saltier water is pushed toward the southern BoB (Figures 7 and 8). The model results show the formation of a sharp frontal boundary near 82°E. The high-resolution COAMPS simulation produced the sharpest front feature near the surface (Figure 7a). There was a convergence of zonal currents near the equator, where the equatorial zonal flow was about 1 m s^1 and 100 m deep. The resulting convergence appears to form a northeast flow of about 0.5–1 m s^{-1} in the upper 100 m near 82°E-84°E, 4°-5°N (Figures 7 and 8). Those transports were more visible near 50 m depth, where the northward flow was strongest (Figure 8). These modeling results are qualitatively consistent with our limited observations. To the east of the EICC the model subsurface flow fields deviate substantially from observations on 18 December, as both models produced strong zonal flows and weak meridional flows, and their maxima were located at relatively shallow depths (Figure 8) compared to the observations (Figure 3), which show a very strong meridional flow and moderate zonal flow, indicating direction of the flow is different. A layer of high salinity water, located between 50 and 125 m, is associated with the northeastward flow field (Figures 6–8), indicating that the water from the equatorial origin moves into the BoB as a subsurface salinity intrusion.

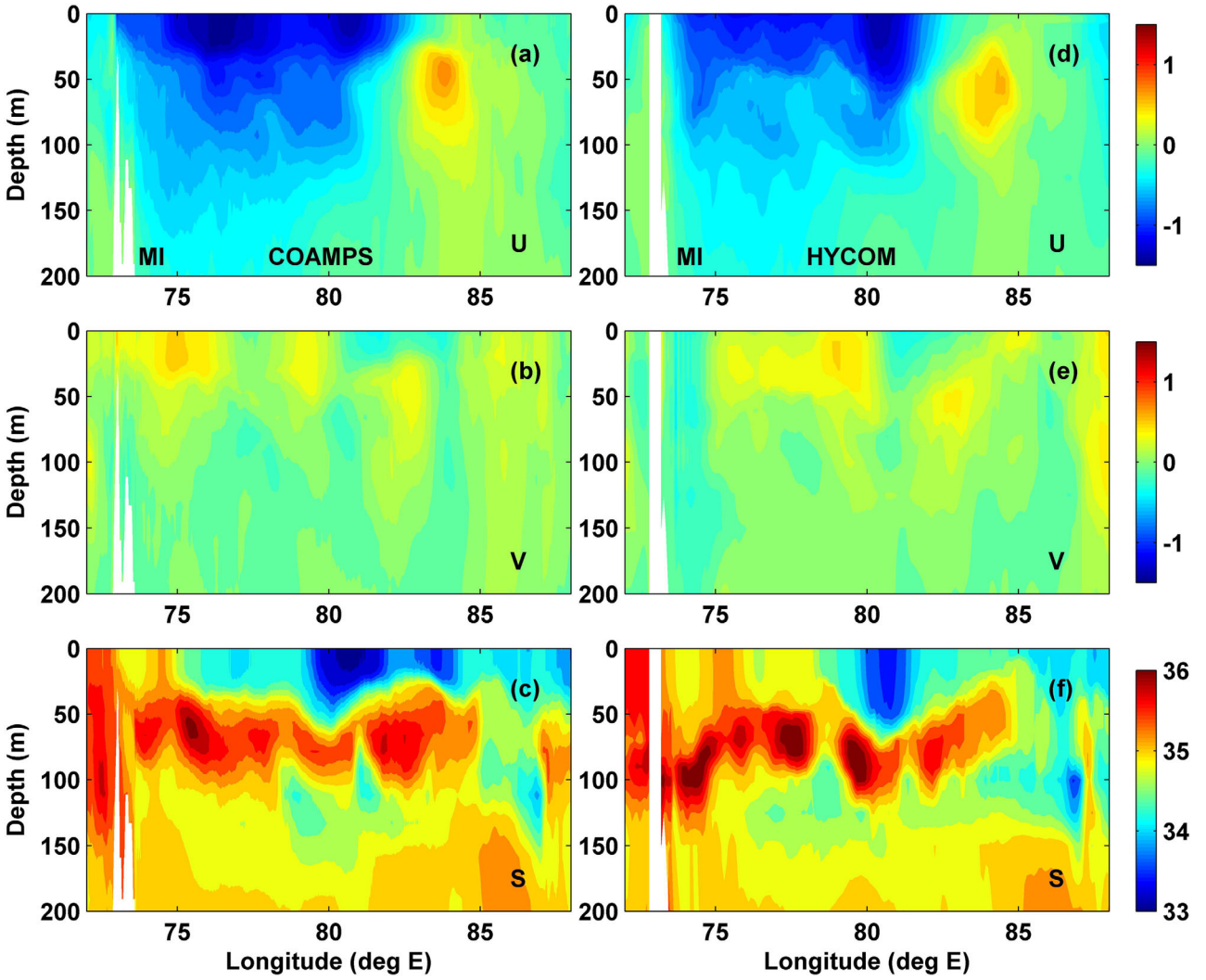

Figure 8. (left) COAMPS (a) zonal velocity, U, (b) meridional velocity, V, and (c) salinity, S along 5.28°N on 18 December 2013. (right) (d) HYCOM U, (e) V, and (f) S. Velocities are in m s^{-1} and salinities are in psu. MI denotes Maldives Island.

3.5. Model-Data Comparisons

The comparison of observations and model results on 18 and 24 December produced mixed results. ADCP, AVISO-drifter, and drifter observations, and COAMPS and HYCOM products along 5.25°N are shown in Figure 9 for comparison. The ADCP currents were at 21 m. The AVISO-drifter currents were estimated at 15 m. The drifters provided currents at 10 m. The model velocities were estimated by averaging daily averaged velocities in the upper 15 m. In general, both the observed and modeled EICC core velocities between 80°E and 81.5°E were comparable. The zonal velocity measured on 18 December is qualitatively consistent with models and AVISO-drifter products, but was underpredicted by both models east of 82.5°E on 24 December (Figures 9a and 9b). On 18 December, both HYCOM and COAMPS underpredicted the observed southward velocity between 81.5°E and 85°E (Figure 9c), while on 24 December, modeled velocities were comparable with the observations (Figure 9d).

Observations and model results showed the presence of a strong boundary current around Sri Lanka in the early stages of the northeast monsoon. Comparisons of observed and model derived boundary currents east and south of Sri Lanka on 18 and 24 December are illustrated in Figures 10 and 11, respectively. Figure 10 shows zonal profiles of meridional currents averaged between7.75°N and 8.25°N, and Figure 11 shows meridional profiles of zonal currents averaged between 80°E and 80.5°E. Drifters, found in those averaging boxes during November and December 2013, were used for the comparison. COAMPS and HYCOM

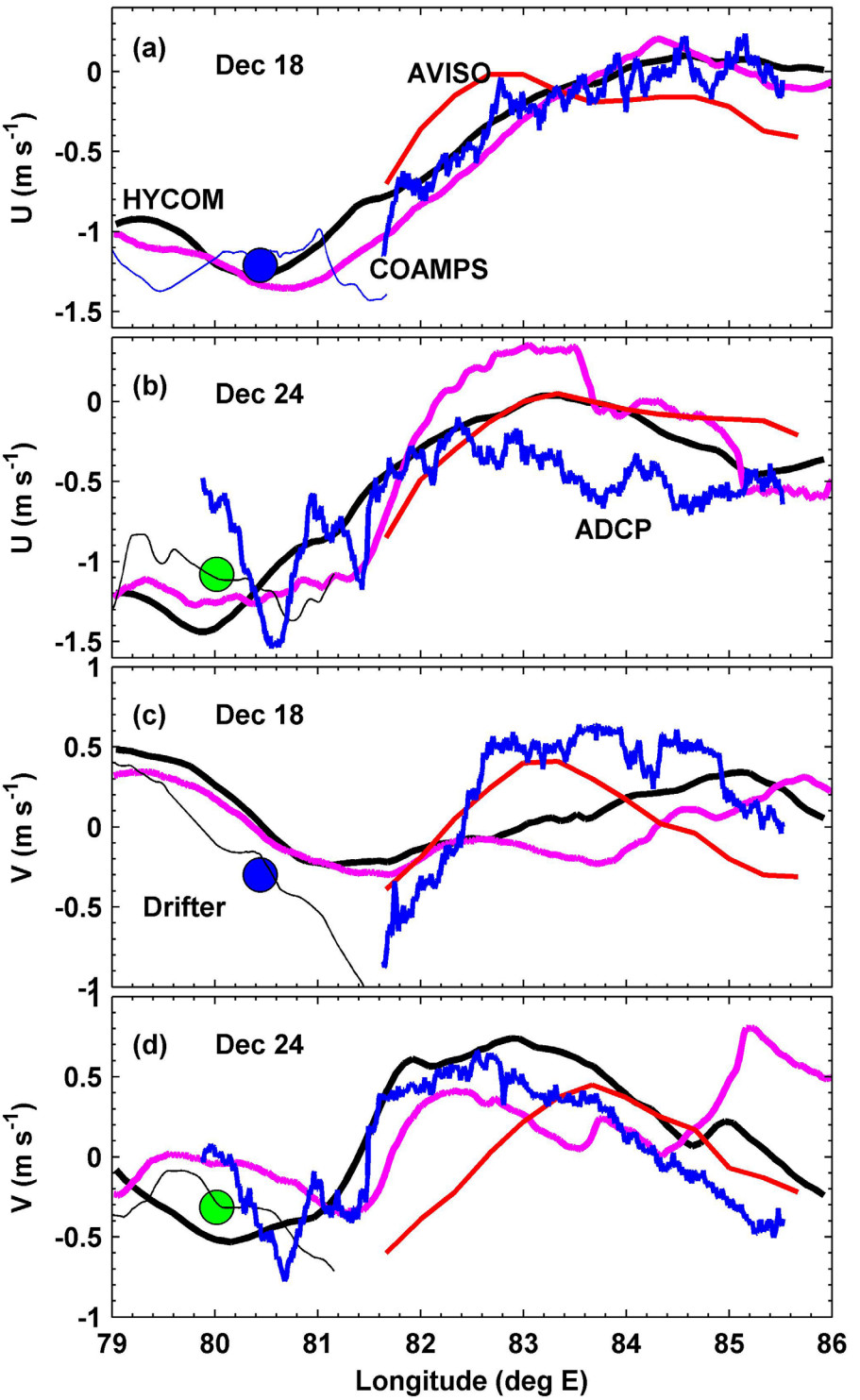

Figure 9. (a, b) U and (c, d) V velocity components along 5.28°E for 18 and 24 December 2013. Red, and blue lines represent velocities from AVISO-drifter at 15 m and ADCP observations at 21 m. Magenta and black lines represent 15 m averaged COAMPS and HYCOM model velocity components. Thin-lines with blue and green bullets denote drifter velocities during 18 and 23 December, respectively.

products and drifter observations were in close agreement at the EICC core, but the modeled currents deviated substantially from the AVISO-drifter currents east of Sri Lanka (Figure 10). The meridional current along 8°N had a jet-like structure similar to a skewed Gaussian-shape function (Figure 10). The jet structure decayed rapidly toward the coast compared to the offshore side. The half-width of the jet was about

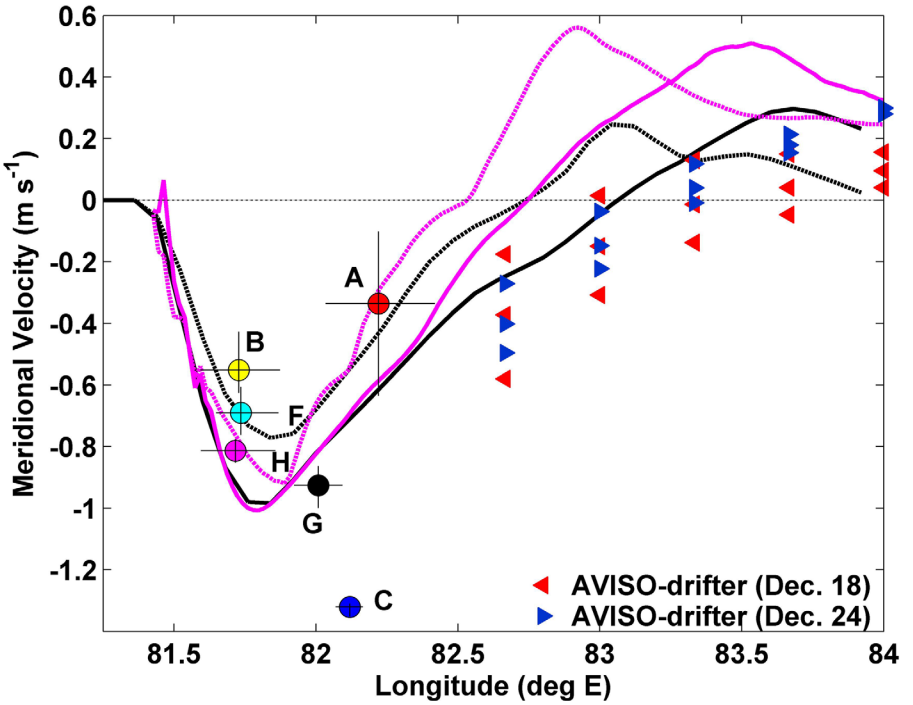

Figure 10. Zonal profiles of V in the upper 15 m to the east of Sri Lanka along 8°N. Solid lines denote daily and meridionally (between 7.25°N and 8.25°N) averaged COAMPS (magenta) and HYCOM (black) velocity for 18 December (solid line) and 24 December 2013 (dashed line). The red and blue triangles denote daily averaged AVISO-drifter velocities within 7.25°N and 8.25°N. Colored circles are drifter velocities within 7.25°N–8.25°N interval for A (29 November), B (3 December), C (16 December), and F-H (24 December) where the time when a given drifter was within 79.9°E–80.6°E, is given inside the parenthesis.

50–75 km. The zonal current south of Sri Lanka also had a jet like structure and was about 200 km wide. In summary, the models capture the boundary current reasonably well, but the interior, subsurface flow has significant differences with observations.

4. Discussion

The dynamics of EICC was studied using a linear, continuously stratified numerical model [e.g., *McCreary et al*., 1996], where four different physical mechanisms were examined: (i) Ekman pumping the interior of the BoB [*Shetye et al*., 1996], (ii) direct forcing by local alongshore winds adjustment to the east coasts of India and Sri Lanka [*McCreary et al*., 1993], (iii) "remote" forcing by alongshore winds adjustment to the northern and eastern boundaries of the bay, [*McCreary et al*., 1993], and (iv) remote forcing from the equator [*Yu et al*., 1991; *Potemra et al*., 1991].

Observations and models results indicate a well-developed EICC flowing equatorward along the eastern boundary of India from 19.5°N to the southern end of Sri Lanka before turning westward. As described above, the EICC was about 100 km wide southeast of India and east of Sri Lanka, and was limited to the upper 200 m. The EICC was 250 km wide to the south and west of Sri Lanka, and the westward flow in the upper 75 m was about 1 m s^{-1}. The southward transports in the upper 200 m at 13°N and 8°N, based on both HYCOM and COAMPS results, were about 5.8–6.8 Sv (1 Sv= 10^6 m^3s^{-1}). These modeled transports are comparable to the estimates made by *Shetye et al*. [1996], who computed geostrophic transport with 1000 dbar as a reference level using hydrographic data collected during December 1991. They reported that the equatorward transport north of 13°N varied between 2.6 and 7.1 Sv, while the transport close to 11°N increased to about 7.7 Sv due to the merging of interior flow just south of 13°N. We noted, based on drifter tracks (Figure 4) that the northwestward flow merged with the coastal current near 15°N, similar to Shetye et al.'s observations.

Both observations and model results showed northward flow east of the EICC (Figures 1, 3, and 5−8). The surface expression of the observed northward flow appeared in a drifter/altimetry synthesis for 18

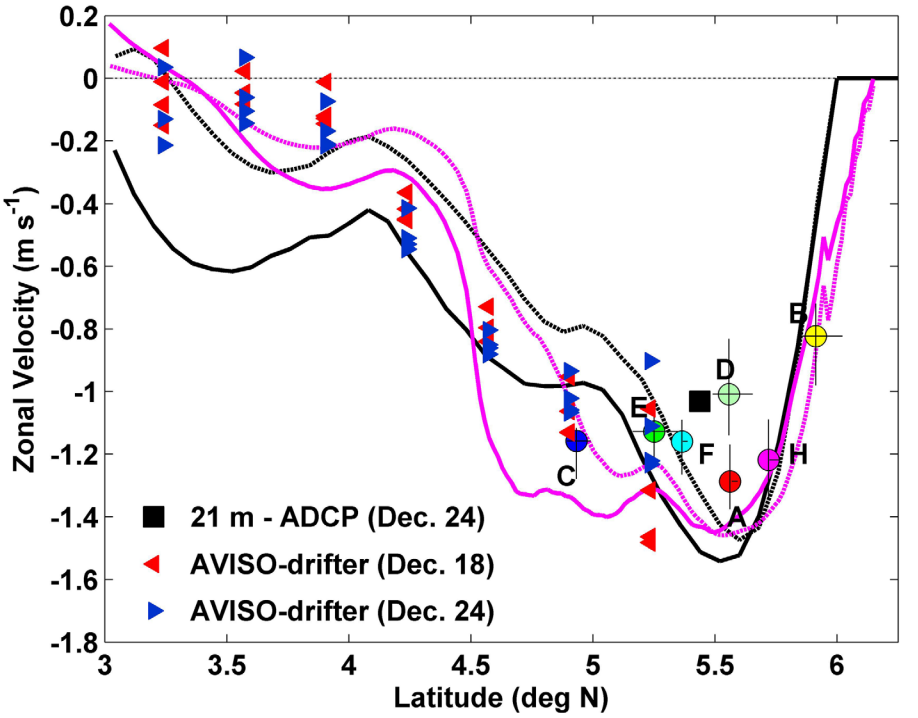

Figure 11. Meridional profiles of U in the upper 15 m to the south of Sri Lanka along 80.25°E. Solid lines denote daily and zonally (between 80°E and 80.5°E) averaged COAMPS (magenta) and HYCOM (black) velocity for 18 December (solid line) and 24 December 2013 (dashed line). The red and blue triangles are AVISO-drifter velocities within 80°E and 80.5°E interval. Colored circles are drifter velocities of A (8 December), B (30 December), C (20 December), D (1 December), E (24 December), F (31 December), and H (29 December) where the time when a given drifter was within 80°E–80.5°E, is given inside the parenthesis. The back square in the right plot denotes the zonal velocity at 21 m water depth from the ship ADCP averaged between 80°E and 80.5°E on 24 December.

December. The subsurface velocity maximum was underpredicted by the models compared to the observations. However, on 23 and 24 December, the northward currents had a two-layer structure consisting of near-surface and subsurface peaks (Figure 3). The HYCOM and COAMPS results captured the basic structure of this flow field (Figure 9d). To evaluate the importance of salt advection into the bay, the meridional transports in the upper 200 m were computed from both observed and modeled velocity fields. The observed transports were estimated by assuming the upper 21 m velocity was uniform and was equal to the velocity at the shallowest depth (21 m) of the ADCP measurements. The transport between 82.5°E and 85.5°E on 18 December was about 22 Sv, and the transport between 81.5°E and 84.5°E on 23 and 24 December was about 11 Sv, indicating a factor of two difference within a week. We note that the observations contained tides, near-inertial, and background internal waves, and that such fluctuations can cause large errors in estimating transport from single velocity sections. The transports from model products were estimated by taking daily and 0.56 degree meridional (i.e., five zonal sections) averages centered at 5.25°N latitude. The corresponding HYCOM transports for 18 and 24 December was about 7.4Sv (±2.5 Sv) and 16.3 Sv (±1.3 Sv), respectively, where the values inside the brackets represent standard deviations. Note HYCOM did not have tides. The transports estimated from COAMPS were about 5Sv and 3 Sv for 18 and 24 December, respectively with large variations due to tides. Differences between observed and model transports and their temporal variations were large. The COAMPS simulations showed that the tidal transports on 18 and 24 December can be as large as ±4 Sv along 5.25°N, and therefore we can expect large uncertainty in our estimates of transport based on observations due to tidal motions. Nevertheless, these estimates indicated that the instantaneous transports were large, and are an important factor for the salt balance in the BoB.

Our observations and numerical predictions show that the northward flow can transport salty water into the southern BoB. An important question is: What are the physical mechanisms for pathways of saltier water during the northeast monsoon? The equatorial jet was formed in December 2013 (http://www7320.nrlssc.navy.mil/GLBhycom1-12/indian.html) and the strongest velocities were found between 50°E and 85°E during a westerly wind pulse in the equatorial Indian Ocean that was connected with a MJO event (http://www.bom.

gov.au/climate/mjo/). The model velocities show that the eastward-flowing surface jet converged with the westward flow near 82°E-85°E, and resulted in a highly time-dependent, complex flow field (Figure 8). One branch of the zonal flow moved northward while carrying high-salinity Arabian Sea-equatorial water, especially at 50–100 m water depths (Figures 3, and 5–9), suggesting a plausible pathway of salt water into the southern BoB during the northeast monsoon. On the other hand, salinity intrusions do not appear to be associated with MJOs in general. In a simulation of three MJO events between 1 October and 31 December, 2011 using COAMPS covering the entire Indian Ocean region [*Jensen et al*., 2015], there was no evidence of strong high-salinity intrusions.

As mentioned in the introduction, during the northeast monsoon the southward EICC is primarily driven by local longshore winds, while interior Ekman pumping drives a surface northward flow near 85°E, with some influence of remote forcing from the equator [*McCreary et al*.,1996]. A northward offshore surface current or upper layer current has been reported during the northeast monsoon by other modeling studies [e.g., *Potemra et al*., 1991; *Yu et al*., 1991; *McCreary et al*., 1993; *Jensen*, 2001]. In *McCreary et al*. [1993], there is an indication of a northward flow below 80 m of a magnitude of about 0.05 m s^{-1} or less. However, the models mentioned above have thick layers and do not include salinity. Direct evidence of a subsurface high-salinity northward flowing intrusion during the northeast monsoon appears to be unreported in the literature. In contrast, such an intrusion has been reported during the southwest monsoon [e.g., *Murty et al*., 1992; *Vinayachandran et al*., 2013] and by models [e.g., *McCreary et al*., 1993; *Vinayachandran et al*., 1999; *Jensen*, 2001, 2003]. Also the southward transport in the EICC during the northeast monsoon is well documented in both models and observations [*Schott and McCreary*, 2001]. Recent analysis of observations found significant variability in the EICC transport on intra-seasonal time scales in the range of 30–90 days [*Durand et al*., 2009; *Mukherjee et al*., 2014]. *Durand et al*. [2009] suggested that intraseasonal fluctuations are driven by remote forcing of the equatorial MJO. Here we report that a subsurface layer of high-salinity water also intrudes into the BoB during the northeast monsoon, while a narrow-band of low-salinity water flushes out of the BoB along the western boundary.

5. Summary

Shipboard current, hydrographic, and meteorological fields were collected during December 2013 as part of the ASIRI-EBOB mooring deployment cruise in the southern BoB. In general, winds were from the northeast with magnitudes of about 2–15 m s^{-1} over the BoB, while a WWB of 5–10 m s^{-1} occurred over the central equatorial IO. The observations captured the EICC which was about 100 km wide with speeds that exceeded 1 m s^{-1} and a northward flow to the east of the EICC which was about 300 km wide with speeds as high as 1 m s^{-1} in the upper 100 m. Combined observations and model results show that the low-salinity BoB water was removed from the bay by the EICC and that high-salinity water was transported into the bay by a northward flow. The model simulations and satellite products suggest that the WWBs can play a significant role in the BoB salinity balance during the northeast monsoon when saltier equatorial water intrudes into the southern BoB via a northward flow. *Vialard et al*. [2009] and *Mukherjee et al*. [2014] show the influence of intraseasonal remote forcing on the interior of the BoB. Our results suggest that direct forcing along the equator may play a significant role for a high-salinity intrusion east of Sri Lanka.

Acknowledgments
This work was sponsored by the ONR in a NRL project referred to as "The Effects of Bay of Bengal Freshwater Flux on Indian Ocean Monsoon (EBOB)." Support for Fernando, Jinadasa, Arulananthan, was provided through ONR grants N00014-13-1-0199 and N00014-14-1-0279. Centurioni was supported by ONR grant N00014-13-1-0477 and NOAA grant "Global Drifter Program" NA10OAR4320156. Assistance provided by the crew of the R/V Roger Revelle was greatly appreciated. Deploying drifters around Sri Lanka by the crew of R/V Samuddrika and NARA technical staff members was greatly appreciated. We also thank Emily Shroyer and Jen Mackinnon for their assistance for the deployment of drifters during the R/V Roger Revelle cruise in November 2014. We also thank three anonymous reviewers for their constructive comments. Observations presented in the manuscript are open-access data. Contact the first author for accessing the data (hemantha.wijesekera@nrlssc.navy.mil).

References

Anderson, D. L. T., and P. B. Rowlands (1976), The role of inertia-gravity waves and planetary waves in the response of a tropical ocean to the incidence of an equatorial Kelvin wave on a meridional boundary, *J. Mar. Res.*, *34*, 295–312.

Booij, N., R. C. Ris, and L. H. Holthuijsen (1999), A third-generation wave model for coastal regions, Part I: Model description validation, *J. Geophys. Res.*, *104*, 7649–7666.

Cane, M. A., and E. S. Sarachik (1977), Forced baroclinic ocean motions: II. The linear equatorial bound case, *J. Mar. Res.*, *35*(2), 395–432.

Centurioni, L. R., J. C. Ohlmann, and P. P. Niiler (2008), Permanent meanders in the California Current System, *J. Phys. Oceanogr.*, *38*(8), 1690–710.

Chi, N-H, R-C Lien, E. A. D'Asaro, and B. B. Ma (2014), The surface mixed layer heat budget from mooring observations in the central Indian Ocean during Madden-Julian Oscillation events, *J. Geophys. Res. Oceans*, *119*, 4638–4652, doi:10.1002/2014JC010192.

Cutler, A.N., and J. C. Swallow (1984), Surface currents of the Indian Ocean (to 25°S, 100°E): Compiled from historical data archived by the Meteorological Office, Bracknell, UK, *Rep. 187*, 36 charts, Inst. of Oceanogr. Sci., Wormley, U. K.

Daley, R., and E. Barker (2001), NAVDAS formulation and diagnostics, *Mon. Weather Rev.*, *129*, 869–883.

Durand, F., D. Shankar, F. Birol and S. S. C. Shenoi (2009), Spatiotemporal structure of the East India Coastal Current from satellite altimetry, *J. Geophys. Res.*, *114*, C02013, doi:10.1029/2008JC004807.

Fox, D. N., W. J. Teague, C.N. Barron, M. R. Carnes, and C. M. Lee (2002), The Modular Ocean Data Assimilation System (MODAS), *J. Atmos. Oceanic Technol.*, *19*, 240–252, doi:10.1175/1520-04267.
Han, W., and J. P. McCreary (2001), Modeling salinity distributions in the Indian Ocean, *J. Geophys. Res.*, *106*, 859–877.
Helber, R. W., T. L. Townsend, C. B. Barron, J. M. Dastague, and M. R. Carnes (2013), Validation test report for the Improved Synthetic Ocean Profile (ISOP) system, Part I: Synthetic profile methods and algorithm, *Naval Res. Lab. Rep. NRL/MR/7320-13-9364*. [Available at http://www7320.nrlssc.navy.mil/all_pubs.html#2013.]
Iskandar, I., and M. J. McPhaden (2011), Dynamics of wind-forced intraseasonal zonal current variations in the equatorial Indian Ocean, *J. Geophys. Res.*, *116*, C06019, doi:10.1029/2010JC006864.
Jensen, T. G. (2001), Arabian Sea and Bay of Bengal exchange of salt and tracers in an ocean model, *Geophys. Res. Lett.*, *28*, 3967–3970.
Jensen, T. G. (2003), Cross-equatorial pathways of salt and tracers from the north Indian Ocean: Modelling results, *Deep Sea Res., Part II*, *50*, 2111–2127, doi:10.1016/S0967-0645(03)00048-1.
Jensen, T. G., T. Shinoda, S. Chen, and M. Flatau (2015), Ocean response to CINDY/DYNAMO MJOs in air-sea coupled COAMPS, *J. Meteorol. Soc. Jpn.*, doi:10.1251/jmsj-2015-049.
Joseph, S., A. J. Wallcraft, T. G. Jensen, M. Ravichandran, S. S. C. Shenoi, and S. Nayak (2012), Weakening of spring Wyrtki jets in the Indian Ocean during 2006-2011, *J. Geophys. Res.*, *117*, C04012, doi:10.1029/2011JC007581.
Kantha, L. H., and C. A. Clayson (2004), On the effect of surface gravity waves on mixing in the oceanic layer, *Ocean Modell.*, *9*, 101–124.
Knox R. A. (1974), On a long series of measurements of Indian Ocean equatorial currents near Addu Atoll, *Deep Sea Res. Oceanogr. Abstr.*, *23*, 211–221.
Lucas, A. J., et al. (2014), From monsoons to mixing: Air-sea interactions in the Bay of Bengal, *Eos Trans. AGU*, *95*, 269–276.
Madden, R. and P. Julian (1971), Detection of a 40-50 day oscillation in the zonal wind in the tropical Pacific, *J. Atmos. Sci.*, *28*, 702–708.
Madden, R., and P. Julian (1972), Description of global-scale circulation cells in the tropics with a 40-50 day period, *J. Atmos. Sci.*, *29*, 1109–1123.
Martin, P. J. (2000), Description of the Navy Coastal Ocean Model Version 1.0, *NRL Rep. NRL/FR/7322/00/9962*, 45 pp., Stennis Space Cent., Hancock, Miss.
McCreary, J. P., P. K. Kundu, and R. L. Molinari (1993), A numerical investigation of dynamics, thermodynamics and mixed-layer processes in the Indian Ocean, *Prog. Oceanogr.*, *31*, 181–244.
McCreary, J. P., W. Han, D. Shankar, and S. R. Shetye (1996), Dynamics of the East India Coastal Current 2. Numerical solutions, *J. Geophys. Res.*, *101*, 13,993–14,010, doi:10.1029/96JC00560.
McPhaden, M. J., G. Meyers, K. Ando, Y. Masumoto, V. S. N. Murty, M. Ravichandran, F. Syamsudin, J. Vialard, L. Yu, and W. Yu (2009), RAMA: The research moored array for African-Asian-Australian monsoon analysis and prediction, *Bull. Am. Meteorol. Soc.*, *90*, 459–480.
Metzger, E. J., et al. (2014), US Navy operational global ocean and Arctic ice prediction systems, *Oceanography*, *27*(3), 32–43, doi:10.5670/oceanog.2014.66.
Moum, J. N., et al. (2014), Air-sea interactions from westerly wind bursts during the November 2011 MJO in the Indian Ocean, *Bull. Am. Meteorol. Soc.*, *95*, doi:10.1175/BAMS-D-12-00225.1.
Mukherjee, A., et al. (2014), Observed seasonal and intraseasonal variability of the East India Coastal Current on the continental slope, *J. Earth Syst. Sci.*, *123*(6), 1197–1232.
Murty, V. S. N., Y. V. B. Sarma, D. P. Rao, and C. S. Murty (1992), Water characteristics, mixing and circulation in the Bay of Bengal during southwest monsoon, *J. Mar. Res.*, *50*, 207–228.
Nagura, M., and M. J. McPhaden (2010), Wyrtki Jet dynamics: Seasonal variability, *J. Geophys. Res.*, *115*, C07009, doi:10.1029/2009JC005922.
Nagura, M., and M. J. McPhaden (2012), The dynamics of wind-driven intraseasonal variability in the equatorial Indian Ocean, *J. Geophys. Res.*, *117*, C02001, doi:10.1029/2011JC007405.
Niiler, P. P., A. Sybrandy, K. Bi, P. M. Poulain, and D. Bitterman (1995), Measurements of the water-following capability of holey-sock and Tristar drifters, *Deep Sea Res., Part I*, *42*, 1951–1964.
O'Brien, J. J., and H. E. Hurlburt (1974), Equatorial jet in the Indian Ocean: Theory, *Science*, *184*, 1075–1077.
Pazan, S. E., and P. P. Niiler (2001), Recovery of near-surface velocity from undrogued drifters, *J. Atmos. Oceanic Technol.*, *18*(3), 476–89.
Philander, S. G. (1990), *El Nino, La Nina and the Southern Oscillation*, 293 pp., Academic, N. Y.
Potemra, J. T., M. E. Luther, and J. J. O'Brien (1991), The seasonal circulation of the upper ocean in the Bay of Bengal, *J. Geophys. Res.*, *96*, 12,667–12,683.
Ralph, E. A., and P. P. Niiler (1999), Wind-driven currents in the tropical Pacific, *J. Phys. Oceanogr.*, *29*(9), 2121–2129.
Rao, R. R., R. L. Molinari, and J. F. Festa (1989), Evolution of the climatological near-surface thermal structure of the tropical Indian Ocean: Description of mean monthly mixed layer depth, and sea surface temperature, surface current, and surface meteorological fields, *J. Geophys. Res.*, *94*, 10,801–10,815.
Schott, F., and J. P. McCreary (2001), The monsoon circulation of the Indian Ocean, *Prog. Oceanogr.*, *51*, 1–123.
Schott, F., J. Reppin, and J. Fisher (1994), Currents and transports of the Monsoon Current south of Sri Lanka, *J. Geophys. Res.*, *99*, 25,127–25,141.
Shankar, D., P. N. Vinayachandran, and A. S. Unnikrishnan (2002), The monsoon currents in the north Indian Ocean, *Prog. Oceanogr.*, *52*, 63–120.
Shetye, S. R., A. D. Gouveia, D. Shankar, S. S. C. Shenot, P. N. Vinayachandran, D. Sundar, G. S. Michael, and G. Nampoothiri (1996), Hydrography and circulation in the western Bay of Bengal during the northeast monsoon, *J. Geophys. Res.*, *101*, 14,011–14,025.
Vialard J, S. S. C. Shenoi, J. P. McCreary, D. Shankar, F. Durand, V. Fernando, and S. R. Shetye (2009), Intraseasonal response of the northern Indian Ocean coastal waveguide to the Madden–Julian Oscillation, *Geophys. Res. Lett.*, *36*, L14606, doi:10.1029/2009GL038450.
Vinayachandran, P. N., Y. Masumoto, T. Mikawa, and T. Yamagata (1999), Intrusion of the Southwest Monsoon Current into the Bay of Bengal, *J. Geophys. Res.*, *104*, 11,077-11,085.
Vinayachandran, P. N., D. Shankar, S. Vernekar, K. K. Sandeep, P. Amol, C. P. Neema, and Abhisek Chatterjee (2013), A summer monsoon pump to keep the Bay of Bengal salty, *Geophys. Res. Lett.*, *40*, 1777–1782, doi:10.1002/grl.50274.
Wyrtki, K. (1973), An equatorial jet in the Indian Ocean, *Science*, *181* (4096), 262–264.
Yoshida, K. (1959), A theory of the Cromwell Current (the equatorial undercurrent) and of the equatorial upwelling––An interpretation in a similarity to a coastal circulation, *J. Oceanogr. Soc. Jpn.*, *15*, 159–170.
Yu, L., J. J. O'Brien, and J. Yang (1991), On the remote forcing of the circulation in the Bay of Bengal, *J. Geophys. Res.*, *96*, 20,449-20,454.
Zhang, C. (2005), Madden-Julian Oscillation, *Rev. Geophys.*, *43*, RG2003, doi:10.1029/2004RG000158.